https://doi.org/10.5194/acp-2021-494
Preprint. Discussion started: 18 June 2021

Atmospheric Chemistry and Physics Discussions

The outflow of Asian biomass burning carbonaceous aerosol into the UTLS in spring: Radiative effects seen in a global model

Prashant Chavan[1,2], Suvarna Fadnavis[1*], Tanusri Chakroborty[1], Christopher E. Sioris[3], Sabine Griessbach[4], Rolf Müller[5]
[1]Indian Institute of Tropical Meteorology, Center for climate change, MoES, India
[2]Savitribai Phule Pune University, Pune, India
[3]Air Quality Research Division, Environment and Climate Change, Toronto, Canada
[4]Forschungszentrum Jülich GmbH, Jülich Supercomputing Center, Jülich, Germany,
[5]Forschungszentrum Jülich GmbH, IEK7, Jülich, Germany
Corresponding author email: suvarna@tropmet.res.in

Abstract

Biomass burning (BB) over Asia is a strong source of carbonaceous aerosols during spring. From ECHAM6-HAMMOZ model simulations and satellite observations, we show that there is an outflow of Asian BB carbonaceous aerosols into the Upper Troposphere and Lower Stratosphere (UTLS) (black carbon: 0.1 to 4 ng m^{-3} and organic carbon: 0.6 to 9 ng m^{-3}) during the spring season. The model simulations show that the greatest transport of BB carbonaceous aerosols into the UTLS occurs from the Indochina and East Asia region by deep convection over the maritime continent that extends to the Bay of Bengal and the South China Sea. The increase in BB carbonaceous aerosols enhances atmospheric heating by 0.002 to 0.02 K day^{-1} in the UTLS. The aerosol-induced heating and circulation changes increase the water vapour mixing ratios in the upper troposphere (20-80 ppmv) and in the lowermost stratosphere (0.02-0.3 ppmv) over the tropics. Once in the lower stratosphere, water vapour is further transported to the South Pole by the lowermost branch of Brewer-Dobson circulation. These aerosols enhance the in-atmosphere radiative forcing (0.68±0.25 W m^{-2} to 5.30±0.37 W m^{-2}), exacerbating atmospheric warming but produce cooling effect on climate (TOA: -2.38±0.12 W m^{-2} to -7.08±0.72 W m^{-2}). The model simulations also show that Asian carbonaceous aerosols are transported to the Arctic in the troposphere. The maximum enhancement in aerosol extinction is seen at 400 hPa (by 0.0093 km^{-1}) and associated heating rates at 300 hPa (by 0.032 K day^{-1}) at the Arctic.

https://doi.org/10.5194/acp-2021-494
Preprint. Discussion started: 18 June 2021

Atmospheric Chemistry and Physics Discussions

1. Introduction

There is growing concern about increasing aerosol amounts over South and East Asia not only because of its contribution to air pollution and its harmful health effects (Chen et al., 2017; Thomas et al., 2019) but also because of its impact on the hydrological cycle (Meehl et al., 2008). Biomass burning (BB) accounts for ~60% of the total aerosol optical depth (AOD) globally (Cheng et al., 2009; Streets et al., 2003). It is one of the major sources of a large carbonaceous aerosol loading. BB is responsible for the major fraction of global mean emissions of black carbon (BC, ~59%) and organic carbon (OC, ~85%) (Bond et al., 2013).

In Asia, China (25%) is the largest contributor to the global BB, followed by India (18%), Indonesia (13%), and Myanmar (8%) (Streets et al., 2003). Among the sources, forest burning (anthropogenic and natural) contributes 45%, burning of crop residues in the field 35%, and burning grassland and savannah 20% to the total BB aerosols in Asia (Streets et al., 2003). Asia emits a substantial amount of BC (~ 0.45 Tg yr^{-1}) and OC (~3.3 Tg yr^{-1}) from BB (Streets et al., 2003). These are significant fractions of the global BB emissions of BC (~2.8–4.9 Tg yr^{-1}) and OC (~31–36 Tg yr^{-1}), respectively (Andreae, 2019). Recently, Wu et al. (2018) and Singh et al. (2020) reported ~83% of the carbonaceous aerosol mass is emitted from open fires over South and East Asia. Within Asia, BB carbonaceous aerosol emissions from East Asia (BC:110 Gg, OC:730 Gg) are larger than over India (BC:83 Gg, OC:650 Gg) and the Indochina region (BC:40 Gg, OC:310 Gg) (Streets et al., 2003).

Biomass burning over Asia shows a strong seasonal cycle peaking in spring (Streets et al., 2003). Our analysis of MODIS fire counts over Asia also shows a pronounced peak in

https://doi.org/10.5194/acp-2021-494
Preprint. Discussion started: 18 June 2021


Atmospheric Chemistry and Physics Discussions

spring (Fig. 1a). The carbonaceous aerosols emitted from BB also peak in spring over Indochina, South Asia, and East Asia regions (Fig. 1b). These aerosols will affect the regional radiative forcing. The literature shows that aerosols emitted from BB in spring produce a significant negative radiative forcing at the top of the atmosphere (TOA) and at the surface, but in-atmospheric radiative forcing (TOA - Surface) is positive over Asia (Wang et al., 2007; Lin et al., 2014; Singh et al., 2020).

Deep convection occurs over the Bay of Bengal and the South China Sea during the spring and monsoon seasons (Randel et al., 2010; Fadnavis et al., 2013; Murugavel et al., 2012) that may transport Asian boundary layer pollutants to the UTLS. Numerous airborne measurements show evidence of carbonaceous aerosol in the upper troposphere over Asia and adjoining outflow regions during spring and monsoon seasons, e.g., measurements from the Civil Aircraft for Regular Investigation of the Atmosphere Based on an Instrument Container (CARIBIC) campaign in 2004, StratoClim in 2017, A-FORCE in 2009, and Transport and Chemical Evolution over the Pacific (TRACE-P) in 2001 (Nguyen et al., 2008; Oshima et al., 2012; Weigel et al., 2020). There may be a significant contribution from BB to the observed carbonaceous aerosols in the UTLS since BB account for ~59-80 % of the carbonaceous aerosols globally (Bond et al., 2013) and being fine-grained, these aerosols have long atmospheric residence times. Transport of Australian wildfire smoke into the stratosphere (~35km) is seen in satellite observations (Khaykin et al., 2020). The balloon-borne, lidar, and satellite observations showed pyro-cumulonimbus events that injected smoke from Canadian forest fires into the stratosphere in August 2017 (Peterson et al., 2018; Hooghiem et al., 2020; Lestrelin et al., 2021). The carbonaceous aerosols were transported to the upper troposphere and produced significant heating locally (Fadnavis et al., 2017). The heating of the upper

https://doi.org/10.5194/acp-2021-494
Preprint. Discussion started: 18 June 2021


Atmospheric Chemistry and Physics Discussions

troposphere induces amplification of vertical motion in the troposphere (Fadnavis et al., 2017; Hooghiem, et al., 2020).

Numerous studies show the transport of boundary layer aerosols from Asia to the lower stratosphere during the monsoon season (Randel et al., 2010; Fadnavis et al., 2013). However, transport of Asian aerosol pollution into the UTLS during the spring season is not reported hitherto when the deep convection occurs over the Bay of Bengal and South China Sea (Fadnavis et al., 2011), and when biomass burning aerosol emissions show a peak (Streets et al., 2003; Fig. 1). In this study, we address these unexplored science questions (1) transport pathways of Asian BB aerosols to the lower stratosphere during the spring season, (2) impacts of Asian BB carbonaceous aerosols on the lower stratosphere. For this purpose, we employ a state-of-the-art ECHAM6-HAMMOZ chemistry-climate model. The model is evaluated against satellite measurements (MODIS and AERONET). The paper is organized as follows: satellite data and the experimental set-up are described in section 2. Section 3 comprises a discussion on the distribution of fires and model evaluation; results are discussed in section 4; conclusions are given in section 5.

2. Model simulations and satellite observations

2.1 Model description and experimental set-up

The fully coupled chemistry-climate model ECHAM6.3–HAM2.3 is used in this study. It comprises the general circulation model ECHAM6 coupled to the aerosol sub-module "Hamburg Aerosol Model (HAM)" (Stier et al., 2005). HAM predicts the evolution of sulfate (SU), BC, OC, particulate organic matter (POM), sea salt (SS), and mineral dust (DU) aerosols. The size distribution of the aerosol population is described by seven lognormal

https://doi.org/10.5194/acp-2021-494
Preprint. Discussion started: 18 June 2021

modes with prescribed variance in the aerosol module (Stier et al., 2005). The anthropogenic and fire emissions of SO_2, BC, and OC are based on the AEROCOM-ACCMIP-II emission inventory. The anthropogenic emissions and fossil fuel sources are based on Lamarque et al., (2010). The biomass burning emissions are from GICC (Mieville et al. 2010), RETRO (Schultz et al., 2008), and GFED v2 (Van Der Werf et al., 2006). The biomass burning emissions for forest and grass fires in this emission dataset represent average conditions of the 2010-2020 period. It should be noted that inter-annual variability of biomass burning is not considered in our simulations. Injection heights of biomass burning emissions are documented by Val Martin et al. (2010). The majority (75%) of the emissions are evenly distributed within the planetary boundary layer (PBL) with 17% in the first level and 8% in the second level above the PBL (Tegen et al., 2019). Biogenic emissions are derived from MEGAN (Guenther 1995). In the model, biogenic OC is directly inserted via emissions. Secondary organic aerosol (SOA) emissions are as described by Dentener et al. (2006). The emissions of sea salt and dust are computed interactively (Tegen et al., 2019).

The model simulations are performed at a T63 spectral resolution corresponding to 1.875º×1.875º in the horizontal resolution, while 47 hybrid σ-p levels provide the vertical resolution from the surface up to 0.01 hPa. The model has 12 vertical levels in the UTLS (300 to 50 hPa). The simulations have been carried out at a time step of 20 min. Atmospheric Model Inter-comparison Project (AMIP) sea surface temperature (SST) and sea ice cover (SIC) were used as lower boundary conditions. We performed 10-member ensemble runs by varying the initial conditions (both SST and SIC) starting between 1 and 10 January 2012 and ending on 31 December 2013 to explore the variability due to the initial conditions. The analysis is performed for the spring season in 2013, leaving the year 2012 for spin-up. The uncertainty estimates in simulated radiative forcing, heating rates, aerosol extinction

https://doi.org/10.5194/acp-2021-494
Preprint. Discussion started: 18 June 2021


Atmospheric Chemistry and Physics Discussions

129 coefficient are obtained from the 10 members of the different initial conditions. The year
130 2013 was chosen for the analysis as this was a neutral year (no El Niño or Indian Ocean
131 Dipole). We performed two sets of 10-member emission sensitivity experiments; in one set of
132 simulations, we switched off biomass burning carbonaceous aerosol emissions (BC and OC).
133 These are referred to as BMaerooff simulations. In another set of simulations, the aerosol
134 emissions from biomass burning were kept on (referred to as BMaeroon simulations).
135
136 **2.2 MODIS fire counts and aerosol optical depth**
137
138 In order to study spatio-temporal variations in the biomass burning activity, we
139 analyze the retrieved daily active fire counts from the Moderate Resolution Imaging
140 Spectroradiometer (MODIS) (https://firms.modaps.eosdis.nasa.gov/download/) onboard
141 Terra and Aqua (Earth Observing System) . MODIS collection-6, Level-2 (combined Aqua
142 and Terra) global monthly fire product mcd14dl at 1 km resolution provides information
143 about the geographic location of the fire and its intensity (Giglio, 2015). The fire detection
144 algorithm uses the strong mid-infrared (IR) emissions from the fires (Matson and Dozier
145 1981) and is based on the brightness temperatures derived from MODIS at the 4 and 11-µm
146 channels. The retrieval algorithm classifies fire pixels in three categories: low confidence (0–
147 30 %), nominal confidence (30–80 %), and high confidence (>80 %). This confidence limit
148 allows the rejection of false fires (Giglio, 2015). Here, data with high or nominal confidence (
149 ≥70 %) are used
150
151 For information on aerosol, we used monthly mean data from MODIS Terra (MOD08
152 M3 V6.1) at 1°×1° horizontal resolution to study AOD variability over the Asian region
153 during spring 2013. MODIS Terra measures radiance emanating from the surface and the

https://doi.org/10.5194/acp-2021-494
Preprint. Discussion started: 18 June 2021

atmosphere and provides images in 36 spectral bands between 0.415 and 14.235 µm, with spatial resolution varying from 250 m to 1 km (Mhawish et al., 2019). Terra MODIS MOD08_M3 (V6.1) aerosol products (i.e., AOD) are retrieved using the Deep Blue (DB) algorithm. The algorithm calculates the column aerosol loading at 0.55 µm over land and ocean.

2.3 Multi-Angle Imaging Spectroradiometer (MISR), Aerosol Robotic NETwork (AERONET) and Optical Spectrograph and InfraRed Imaging System (OSIRIS) observations

The AOD retrievals from Multi-Angle Imaging Spectroradiometer (MISR) at 550 nm wavelength and Aerosol Robotic NETwork (AERONET) sunphotometer during spring 2013 are also used for comparison with the model simulations. Details of MISR are available at https://misr.jpl.nasa.gov/getData/accessData/ and AERONET at https://aeronet.gsfc.nasa.gov/. AERONET AOD observations are obtained at different stations in the Indochina region (Myanmar: 16.86°N-96.15°E, Vientiane: 17.99°N-102.57°E, Siplakorn University: 13.81°N-100.04°E, Ubon-Ratchathani: 15.24°N - 104.87°E), South Asia (Gandhi college: 25.81°N - 85.12°E, Kathmandu Bode: 27.68°N,-85.39°E, Dhaka University: 23.72°N-90.39°E), East Asia (Nghia-Do: 21.04°N-105.80°E, Hong Kong Polytechnic University: 22.30°N-114.18°E).

We compared simulated aerosol extinction coefficient vertical profile with observations from Optical Spectrograph and InfraRed Imaging System (OSIRIS) on-board the Odin satellite (Bourassa et al., 2007). We used version 7.0 vertical profiles of aerosol extinction at 750 nm for March-May 2013 (https://research-groups.usask.ca/osiris/data-

https://doi.org/10.5194/acp-2021-494
Preprint. Discussion started: 18 June 2021

179 products.php#Download). The limb scatter measurements from OSIRIS show good
180 agreement with Stratospheric Aerosol and Gas Experiment (SAGE) II and Scanning Imaging
181 Absorption spectrometer for Atmospheric Chartography (Rieger et al., 2018). We also
182 analyzed Outgoing Longwave Radiation (OLR) data for March-May 2013 from
183 National Center for Environmental Prediction (NCEP) re-analysis-2
184 (https://psl.noaa.gov/data/gridded/data.ncep.reanalysis2.pressure.html).
185
186 **3. Distribution of fires and model evaluation**
187 **3.1 Seasonal distribution of fires over Asia**
188
189 In this section, we discuss the seasonal variability of fire activity in Asia. The fire
190 counts peak over Asia (10°S-50°N, 60°E-130°E) in the spring season. Figure 1a-b shows that
191 fires are clustered over three sub-regions (1) Indochina region (91ºE - 107ºE, 10ºN - 27 ºN)
192 (numbers of fire counts: 80694), (2) East Asia (108ºE - 123ºE, 22ºN - 32ºN), (numbers of fire
193 counts: 4770), (3) South Asia (65°E - 90°E, 80°N - 32°N) (numbers of fire counts: 14223)
194 (Fig. 1b). Fire counts over the three sub-regions peak in spring although the month varies,
195 e.g., fire counts over East Asia show a peak in March, Indochina region in March-April, and
196 South Asia in May (Fig. 1a). The fire counts over South Asia show a secondary peak in
197 October. In agreement with our results, Bhardwaj et al. (2016) also reported high fire activity
198 in spring and the lowest fire activity in monsoon (June–September) during 2003-2013. Streets
199 et al. (2003) reported that higher fire counts during the spring season over South Asia and
200 East Asia are attributed to enhanced crop burning activity. Over the Indochina region, high
201 fire counts are associated with forest fires along with crop burning. Intense biomass burning
202 activity over Asia during the spring season is also reported by Zhang et al. (2020). Hence, we
203 provide further analysis in spring.

https://doi.org/10.5194/acp-2021-494
Preprint. Discussion started: 18 June 2021


Atmospheric Chemistry and Physics Discussions

204 **3.2. Model evaluation**

205

206 We compare simulated seasonal mean (BMaeroon) AOD with MODIS, MISR, and
207 AERONET. Figure 2 (a-c) shows large AOD over the regions: Indochina (MODIS: ~0.4 to
208 0.8, MISR: 0.27 to 0.6; model: 0.27 to 0.5), East Asia (MODIS: 0.5 to 1.3, MISR: 0.27 to 1,
209 model: 0.5 to 1.4), and the Indo-Gangetic plain in south Asia (23ºN -30ºN, 75ºE -85ºE)
210 (MODIS: 0.24 to 0.8, MISR: 0.24 to 0.5, model: 0.3 to 0.6). The MISR AOD is
211 comparatively less than MODIS AOD over all three study regions (Fig. 2a-b). There are
212 differences in spatial distribution of AOD among MODIS, MISR and the model. Over East
213 Asia, the model overestimates AOD relative to MISR (by 0.24) and MODIS (by 0.1). Over
214 Indochina, the model shows an underestimation compared to MISR (by 0.1) and MODIS (by
215 0.2). The simulated AOD is over-estimated over the Indo-Gangetic plain in comparison with
216 MISR (by 0.08) and under-estimated compared to MODIS (0.2). Tegen et al. (2019) also
217 reported that in ECHAM6–HAMMOZ simulations the AOD is overestimated over East Asia
218 in comparison with MISR.

219

220 Further, we compare simulated AOD with ground-based measurements at ten
221 AERONET stations during spring 2013 (Figure 2d). Model results were sampled at each
222 station at the same time. Comparison with AERONET observations also shows that the
223 model underestimates AOD over all the stations. The simulated AOD (0.54) shows the
224 highest underestimation at Nghia Do (21.04°N - 105.80°E) in East Asia and the lowest
225 underestimation at Gandhi college (25.81°N - 85.12°E) in the Indo-Gangetic plain, where the
226 simulated 550 nm AOD is 0.57. The differences in the magnitude of AOD between model,
227 satellite remote sensing (MISR, MODIS), and ground-based AERONET observations may be
228 caused by various factors; e.g., satellite remote sensing of AOD exhibits biases over certain

https://doi.org/10.5194/acp-2021-494
Preprint. Discussion started: 18 June 2021


Atmospheric Chemistry and Physics Discussions

surface types. There are further uncertainties in the model emission inventories (Fadnavis et al., 2013, 2017, 2019).

The vertical distribution of simulated aerosol extinction coefficient profiles (BMaeroon) averaged over the BB burning region (10ºN-30ºN) are compared with OSIRIS observations (Fig 2e-f). Our model could simulate vertical variations similar to those observed by OSIRIS. A plume rising from 90ºE-120ºE extends to 16 km is also evident in the OSIRIS data although the model underestimates the aerosol extinction coefficient by 0.0002 - 0.0003 km^{-1}. This underestimation may be due to uncertainties in the model due to emission inventory and transport processes in the model. There may be further biases in OSIRIS measurements due to assumptions made on the aerosol size distribution and chemical composition (Bourassa et al., 2012).

4. Results

4.1 Impact of biomass burning on Aerosol Optical Depth (AOD)

Figure 3 (a) shows the distribution of anomalies in simulated AOD (BMaeroon-BMaerooff). It shows enhanced AOD anomalies over Indo-Gangetic plain (~0.22 to 0.8), the Tibetan Plateau and parts of East Asia (~0.3 to 1.2). Past studies show that a large amount of dust is transported from west Asia to the Indo-Gangetic plain and Tibetan Plateau region (Lau and Kim 2006; Fadnavis et al., 2017). The distribution of simulated dust AOD also indicates an enhancement over the Indo-Gangetic plain and Tibetan Plateau region (Fig 3b). It may be due to dynamical changes induced by the carbonaceous aerosol that enhanced dust transport to the Indo-Gangetic plain and Tibetan Plateau region. A large value of dust AOD over the Indo-Gangetic plain, Tibetan Plateau, and Mongolian desert is seen in Fig 3b. The influence

https://doi.org/10.5194/acp-2021-494
Preprint. Discussion started: 18 June 2021


Atmospheric Chemistry and Physics Discussions

of BB carbonaceous aerosol on the AOD is evident when dust AOD is not considered (Fig.3c, positive anomalies over Indo-China, South Asia, and East Asia).

Figure 3d shows the spatial distribution of the AOD for carbonaceous aerosols (BC+OC). The changes in concentration of total column carbonaceous aerosols are shown in Fig. S1a. Figures 3d and Fig. S1a show increases in aerosols over Indochina (AOD: +0.04-0.07, concentration: +40-80%), Indo-Gangetic plain (AOD: +0.014-0.03, concentration: +10-50%) and East Asia (AOD: +0.018-0.04, concentration: +20-60%). It is evident that anomalies of carbonaceous aerosols AOD over the Indo-Gangetic plain and East Asia are comparatively lower than over the Indochina region. In agreement with our results, Wang et al. (2015) also reported an abundant mixture of BC and OC particles due to BB over the Indochina region in spring 2014. Our model simulations show that the contribution of BB-emitted OC to AOD (Indochina 16 to 35 %; East Asia: 4 to 12 %; South Asia: 0.8 to 4 %) is higher than that of BB-emitted BC (Indochina: 1.8 to 6 %; East Asia: 0.8 to 1.4 %; South Asia: 0.2 to 0.8 %) (Fig. S1b-c). Figure 3d also shows high amounts of carbonaceous aerosols over the western Pacific, which may be due to transport from the Indochina region by westerly winds (discussed later in subsection 4.3).

4.2. Impact of BB carbonaceous aerosol on radiative forcing

The carbonaceous aerosols emitted from biomass burning may significantly change radiative forcing by absorption and attenuation of solar and terrestrial radiation (Schill et al., 2020). The seasonal mean anomalies in net radiative forcing show negative radiative forcing at the surface and top of the atmosphere (TOA) over South Asia (surface: -5.08±0.44 W m^{-2}; TOA: -4.39±0.26 W m^{-2}), Indochina region (surface:-7.68±0.45 W m^{-2}; TOA:-2.38±0.12 W

https://doi.org/10.5194/acp-2021-494
Preprint. Discussion started: 18 June 2021

279 m^{-2}) and East Asia (surface:-10.81±0.63 W m^{-2}; TOA: -7.08±0.74 W m^{-2}) (Fig. 4). The
280 estimates of in-atmosphere radiative forcing show positive anomalies over south Asia
281 (0.68±0.25 W m^{-2}), Indochina region (5.30±0.37 W m^{-2}), and East Asia (3.73±0.20 W m^{-2}),
282 indicating an atmospheric warming. In agreement with our study, a number of studies showed
283 a negative radiative impact at the TOA and surface, but positive in-atmosphere radiative
284 forcing due to BC and OC aerosols over the Indochina region. For example, Lin et al. (2014)
285 reported an radiative forcing of -4.74 W m^{-2} at the TOA, -26.85 W m^{-2} at the surface, thus
286 +22.11 W m^{-2} in-atmosphere. Wang et al. (2007) estimated radiative forcing -1.4 to -1.9 W m^{-2} at TOA and -4.5 to -6 W m^{-2} at the surface, yielding 2.6 W m^{-2} in-atmosphere during March
288 2001. Singh et al. (2020) also reported radiative forcing at TOA -1.91 W m^{-2} and -42.76 W m^{-2} at the surface and 40.85 W m^{-2} in-atmosphere over Myanmar.
290

291 **4.3. Transport of biomass burning aerosol into the upper troposphere and lower**
292 **stratosphere**
293

294 The stepwise evolution of the Asian summer monsoon begins in spring and contributes a
295 significant amount of rainfall to the total annual precipitation over China (25–40%) and over
296 South Asia (~11-20%) due to deep convection over the Bay of Bengal and South China Sea
297 (Guhathakurta and Rajeevan 2008; Li et al., 2016). The distribution of outgoing long-wave
298 radiation (OLR) from NCEP reanalysis data during the spring season confirms that deep
299 convection occurs over the maritime continent that extends to the South China Sea and Bay
300 of Bengal (Fig. 5a). Our model simulation shows a distribution of OLR similar to the
301 observations, although OLR is overestimated in the model (Fig. 5b). Figure 5(c)-(d) shows
302 the combined distribution of Cloud Droplet Number Concentration (CDNC), Ice Crystal
303 Number Concentration (ICNC), and vectors of the resolved circulation, which exhibit a

https://doi.org/10.5194/acp-2021-494
Preprint. Discussion started: 18 June 2021


Atmospheric Chemistry and Physics Discussions

304 strong upwelling in the equatorial Asia (10ºS-10ºN, 80ºE-140°E, Fig. 5c-d). This upwelling
305 associated with deep convection may transport pollutants from the boundary layer into the
306 UTLS.
307
308 We analyzed the vertical distribution of simulated anomalies (BMaeroon -
309 BMaerooff) of BB carbonaceous aerosols obtained over the high fire emission regions, i.e.,
310 Indochina, South Asia, and East Asia in spring 2013 (Fig. 1b). The simulated distribution of
311 BC aerosols (Fig. 6 a-b) and OC aerosols (Fig. 6c-d) over the Indochina region indicates an
312 aerosol plume extending to the lowermost stratosphere. The ascent resolved in the wind
313 vectors together with the distribution of cloud droplets and cloud ice indicate that the
314 transport of these aerosols from the surface to the lowermost stratosphere occurs due to deep
315 convection over the Bay of Bengal and South China Sea (Fig. 5a-b). There is an enhancement
316 of BC aerosol concentration by 0.1 – 1.6 ng m^{-3} (Fig. 6 a-b) and for OC by 0.6 – 6 ng m^{-3}
317 (Fig. 6 c-d) in the UTLS (300 - 90hPa) over the Indochina region.
318
319 In the troposphere, biomass-burning carbonaceous aerosols are transported to the
320 Arctic (Fig. 6a and Fig. 6c). Some previous studies also show aerosol transport from South
321 Asia and East Asia to the Arctic (Shindell et al., 2008; Fisher et al., 2011). The carbonaceous
322 aerosols are also transported towards the Western Pacific (Fig. 6 b-d and 6 f-h). In the Pacific
323 (140ºE-170ºW), these aerosols are lifted to the UTLS. Transport of the aerosols from the
324 Indochina region to the Western Pacific has also been reported in the past (Dong and Fu,
325 2015).
326
327 Further, we show the distribution of BB carbonaceous aerosol over East Asia in
328 Figure 6 e-h. It shows that the plume of BC and OC aerosol crosses the tropopause (BC: 0.4–

https://doi.org/10.5194/acp-2021-494
Preprint. Discussion started: 18 June 2021


Atmospheric Chemistry and Physics Discussions

329 2 ng m^{-3} and OC: 0.6 to 9 ng m^{-3}). Figures 6e and 6g also show that the aerosol plume from
330 the equatorial region is lifted to the UTLS associated with the Indonesian region (130ºE -
331 170ºE). Similar to the Indochina region, BC and OC aerosols also show poleward transport
332 to the Arctic and horizontal transport towards the Western Pacific (Figures 6f and 6h). These
333 aerosols are vertically transported in the western Pacific (130ºE - 170ºE). Distribution of
334 anomalies of BC and OC near the tropopause (at 100 hPa) show outflow of Asian
335 carbonaceous aerosols in the UTLS over equatorial Asia and Western Pacific (5°S-20°N,
336 70°E-180°E) (Fig. S3).
337
338 The BB over South Asia is present over central India (70°E - 90°E, 8°N - 24°N) and
339 occurs in spring (Fig. 1 b and Singh et al., 2017). BC and OC emissions over South Asia
340 during the spring season are reported in many studies (Talukdar et al., 2015; Guha et al.,
341 2015). The vertical distribution of anomalies of BC and OC over south Asia shows that
342 positive anomalies of BC and OC aerosols extend from the surface to the upper troposphere
343 (300 hPa) (Fig. S2). CALIPSO derived aerosol profiles in spring 2013 also show plumes
344 reaching up to approximately 7 km (400 hPa) (Singh et al., 2020). Unlike the Indochina
345 region, BB carbonaceous aerosols over Indo-Gangetic plain do not reach the lowermost
346 stratosphere during the spring season. Hence, hereafter we focus our discussion on the
347 transport of BB carbonaceous aerosols and their impacts on the UTLS for Indochina and East
348 Asia.
349
350 Further, we analyze aerosols enhancement over the Arctic (65ºN - 85ºN) because of the
351 transport of Asian biomass burning BC and OC aerosols. The vertical distribution of
352 anomalies of aerosol extinction shows an enhancement of 0-0.0093 km^{-1} in the Arctic (1000 -

https://doi.org/10.5194/acp-2021-494
Preprint. Discussion started: 18 June 2021


Atmospheric Chemistry and Physics Discussions

100hPa) with a peak at 400 hPa (Fig. 7). Shindell et al. (2008) also showed seasonally varying transport of South Asian aerosols to the Arctic that maximizes in the spring season.

4.4 Impact of BB carbonaceous aerosol on heating rates

Carbonaceous aerosols in the atmosphere produce significant heating leading to atmospheric warming (Fadnavis et al., 2017). We obtained anomalies in heating rates (shortwave+longwave) due to carbonaceous aerosols (BMaeroon - BMaerooff). Figures 8a-d show the vertical distribution of heating rates over the Indochina region and East Asia. It shows that enhanced BB carbonaceous aerosols have induced enhanced heating of the atmospheric column along the pathway through which they are transported (Fig. 5a-h). The carbonaceous aerosol emissions over the Indochina region and East Asia produced anomalous heating of ~0.1 to 0.04 K day^{-1} in the lower troposphere (1000 hPa to 400 hPa) and ~0.006 to 0.002 K day^{-1} near the tropopause (200 hPa to 80 hPa). Figure 6 a, c, e, g shows that descending winds transport BC and OC aerosols from above the tropopause downward and southward to 20°S. The positive anomalies in heating rates of ~0.002 to 0.006 K day^{-1} in the upper troposphere at ~200 hPa near 20ºS may be due to heating by these aerosols. There may be dynamic changes in response to BB carbonaceous aerosol emission. The transported Asian carbonaceous aerosols and associated dynamical changes in the Arctic enhanced heating rates by 0-0.032 K day^{-1} between 1000 - 100 hPa (Fig.7). Also, transport of carbonaceous aerosol to the western Pacific (Fig. 6 b, d, f, h) by the westerly winds has increased heating by 0.008 to 0.02 K day^{-1} and peaks at 250 hPa (0.02 K day^{-1}) over the Central Pacific (170°W - 110°W).

https://doi.org/10.5194/acp-2021-494
Preprint. Discussion started: 18 June 2021


Atmospheric Chemistry and Physics Discussions

Figure 8 (a-d) shows positive anomalies in heating rates at the tropopause. Heating in the upper troposphere enhances the vertical motion that may enhance the transport into the lower stratosphere (Gettelman et al., 2004). Carbonaceous aerosols that cross the tropopause (0.1 to 4 ng m^{-3}) and enter the lowermost stratosphere (Figs. 6 a-h) may be due to increased vertical motion in response to enhanced heating. This shows that aerosols induce positive feedback on vertical transport.

4.5 Impact of BB carbonaceous aerosol on water vapor

The heating produced by the biomass burning carbonaceous aerosols may affect the distribution of water vapor in the troposphere and stratosphere. Figure 9a-b shows anomalies in water vapor (BMaeroon - BMaerooff) over Indochina and East Asia. An interesting feature seen in Fig 9a-b is the enhanced transport of water vapor (an anomaly of 0.02-0.5 ppmv) to the South Pole through the lower stratosphere from Indochina (91°E - 107°E, 10°N - 27ºN) and East Asia (108°E - 123°E, 20°N - 35°N). The tropospheric heating might have caused elevated water vapor injection into the lower-stratosphere. The water vapour in the lower stratosphere is further transported to the South Pole by the lower branch of the Brewer-Dobson circulation. The water vapour reaches the Arctic within a month indicating fast transport.

The model simulations show noticeable enhancement of water vapor (0.4 to 1.6 ppmv) in the northern tropics near the tropopause (150 hPa) and by 0.2-0.7 ppmv in the Arctic lower stratosphere (150 hPa) (Fig. 9c). In the tropical lower stratosphere, it is increased by 0.02-0.3 ppmv (Fig. 9d). Water vapor being a greenhouse gas amplifies global warming leading to positive feedback (e.g., Riese et al., 2012; Sherwood et al., 2018,

https://doi.org/10.5194/acp-2021-494
Preprint. Discussion started: 18 June 2021


Atmospheric Chemistry and Physics Discussions

Fadnavis et al., 2021). The strong negative anomalies of OLR (Fig. S4) induced by carbonaceous aerosols also indicate the positive feedback (Fig. 6). Fadnavis et al. (2013) also reported an increase in water vapor in the UTLS in response to the enhancement of aerosols. Stratospheric water vapor plays a significant role in climate change (e.g., Oman et al., 2008; Wang et al., 2020; Xie et al., 2020).

5. Conclusions

A ten-member ensemble of ECHAM6.3–HAM2.3 simulation for the spring season 2013, an ENSO neutral year, is analyzed to study the transport of carbonaceous aerosol injected by Asian biomass burning into the UTLS and its associated impacts on radiative forcing, heating rates, and water vapor. To validate the model simulations, we compare simulations with observations from (1) MODIS, (2) MISR, (3) AERONET, (4) OSIRIS satellite retrieval during spring 2013. The observational analysis shows reasonable agreement with the model simulations.

The BB emission increases the aerosol burden (AOD) over the Indochina region by 0.14 to 0.22 (carbonaceous aerosol concentration increase of +40-80%), India by 0.22 to 0.38 (concentration of carbonaceous aerosol: +10-50%), and East Asia by 0.18 to 0.26 (concentration of carbonaceous aerosol: +20-60%).Our analysis shows that deep convection, which occurs over the maritime continent that extends to the Bay of Bengal and the South China Sea, during spring plays an important role in transporting Asian BB carbonaceous aerosols to the lowermost stratosphere. The model simulations show that carbonaceous aerosols are transported from the boundary layer of the Indochina and East Asia region into the lowermost stratosphere (BC: 0.1 to 4 ng m^{-3} for BC, OC: 0.4 to 9 ng m^{-3}). In the UTLS,

https://doi.org/10.5194/acp-2021-494
Preprint. Discussion started: 18 June 2021


Atmospheric Chemistry and Physics Discussions

outflow occurs over equatorial Asia and the Western Pacific (10°S - 20°N, 70°E - 180°E). Carbonaceous aerosols originating from Asian biomass burning are also transported to the Arctic. The maximum enhancement in aerosol extinction (by 0.0093 km^{-1}) is seen at 400 hPa at the Arctic.

The enhanced carbonaceous BC and OC aerosol emitted from BB produces a negative net radiative forcing at the surface (India: -5.08±0.44 W m^{-2}, Indochina: -7.68±0.45 W m^{-2}, and East Asia: -10.81±0.63 W m^{-2}), at the TOA (India: -4.39±0.26 W m^{-2} over, Indochina: -2.38±0.12 W m^{-2}, and East Asia: -7.08±0.74 W m^{-2}) and positive net radiative forcing in the atmosphere (India: 0.68±0.25 W m^{-2}, Indochina: 5.30±0.37 W m^{-2}, and East Asia: 3.73±0.20 W m^{-2}) indicating atmospheric warming and cooling of the climate.

The changes in BB carbonaceous aerosol induce a warming in the troposphere (0.008 – 0.1 K day^{-1}) and in the UTLS (~0.002 to 0.006 K day^{-1}) over Asia. The aerosols transported to the Arctic enhance heating by 0 - 0.032 K day^{-1}, peaking at 300 hPa. The outflow of aerosols in the UTLS over the western Pacific by the westerly winds has increased heating by 0.008 to 0.02 K day^{-1}. The atmospheric heating induced by Asian BB carbonaceous aerosols led to the transport of water vapor into the lower stratosphere (0.02-0.3 ppmv) over the tropics. In the lower stratosphere, water vapour is transported to the South Pole by the lower branch of the Brewer Dobson circulation. Water vapor being a greenhouse gas amplifies atmospheric heating, leading to positive feedback (e.g., Riese et al., 2012; Sherwood et al., 2018).

Thus, our analysis also shows that Asian biomass burning carbonaceous aerosols lead to moistening of the troposphere in the northern hemisphere and lowermost stratosphere in

https://doi.org/10.5194/acp-2021-494
Preprint. Discussion started: 18 June 2021


Atmospheric Chemistry and Physics Discussions

452 the northern tropics and southern hemisphere. The enhanced lower stratospheric water vapor
453 affects the stratospheric temperature, resulting in a warming of the lower stratosphere, which
454 is however counteracted by the stratospheric cooling caused by the increase in atmospheric
455 CO_2.
456

https://doi.org/10.5194/acp-2021-494
Preprint. Discussion started: 18 June 2021

457 **Data availability:** The MODIS Fire count data were downloaded from
458 https://firms.modaps.eosdis.nasa.gov/download. The AOD data from MODIS Terra can be
459 downloaded from https://ladsweb.modaps.eosdis.nasa.gov/archive/allData/61/MODATML2/
460 The AOD data from MISR were obtained from
461 https://misr.jpl.nasa.gov/getData/accessData/. The AERONET data were obtained from
462 https://aeronet.gsfc.nasa.gov/. Data of NCEP reanalysis-2 outgoing Long Wave Radiation
463 (OLR) were obtained from
464 https://psl.noaa.gov/data/gridded/data.ncep.reanalysis2.pressure.html. The OSIRIS Aerosol
465 extinction coefficient can be downloaded from https://research-groups.usask.ca/osiris/data-
466 products.php#Download
467 **Author contributions**: S. F. initiated the idea. P. C. and T. C. performed model analysis. R
468 M., S.G and C.E.S. contributed analysis and study design. C. E. S.and S.G. analyzed OSIRIS
469 data. All authors contributed to the writing and discussions of the manuscript.
470 **Competing Interests**: The authors declare no competing interests.
471
472

https://doi.org/10.5194/acp-2021-494
Preprint. Discussion started: 18 June 2021

References:

Andreae, M. O.: Emission of trace gases and aerosols from biomass burning – an updated assessment, Atmos. Chem. Phys., 19, 8523–8546, https://doi.org/10.5194/acp-19-8523-2019, 2019.

Bhardwaj, P. M., Naja, R., Kumar, and H. C., Chandola.: "Seasonal, Interannual, and Long-Term Variabilities in Biomass Burning Activity over South Asia." Environmental Science and Pollution Research 23(5):4397–4410, 2016.

Bond, T. C., S. J. Doherty, D. W., Fahey, P. M., Forster, T., Berntsen, B. J., Deangelo, M. G., Flanner, S., Ghan, B., Kärcher, D., Koch, S., Kinne, Y., Kondo, P., K., Quinn, M., C., Sarofim, M., G., Schultz, M., Schulz, C., Venkataraman, H., Zhang, S., Zhang, N., Bellouin, S., K., Guttikunda, P., K., Hopke, M., Z., Jacobson, J., W., Kaiser, Z., Klimont, U., Lohmann, J., P., Schwarz, D., Shindell, T., Storelvmo, S., G., Warren, and C., S., Zender.: "Bounding the Role of Black Carbon in the Climate System: A Scientific Assessment." Journal of Geophysical Research Atmospheres 118(11):5380–5552, 2013.

Bourassa, A. E., Rieger, L. A., Lloyd, N. D., and Degenstein, D. A.: "Odin-OSIRIS stratospheric aerosol data product and SAGE III intercomparison". Atmos. Chem. Phys., 12, 605–614, https://doi.org/10.5194/acp-12-605-2012, 2012.

Chen, J. C., Li, Z., Ristovski, A., Milic, Y., Gu, M., S., Islam, S., Wang, J., Hao, H., Zhang, C., He, H., Guo, H., Fu, B., Miljevic, L., Morawska, P., Thai, Y., Fat LAM, G., Pereira, A., Ding, X., Huang, and U., C., Dumka.: "A Review of Biomass Burning: Emissions and Impacts on Air Quality, Health and Climate in China." Science of the Total Environment 579(November 2016):1000–1034, 2017.

Cheng, F. Y., Z., M., Yang, Chang Y., and F., Ngan.: "A Numerical Study of the Dependence

https://doi.org/10.5194/acp-2021-494
Preprint. Discussion started: 18 June 2021

498 of Long-Range Transport of CO to a Mountain Station in Taiwan on Synoptic Weather
499 Patterns during the Southeast Asia Biomass-Burning Season." Atmospheric
500 Environment 78:277–90, 2013.
501 Cheng, Y. F., M., Berghof, R., M., Garland, A., Wiedensohler, B., Wehner, T., Müller, H.,
502 Su, Y., H., Zhang, P., Achtert, A., Nowak, U., Poschl, T., Zhu, M., Hu, and L., M.,
503 Zeng.: "Influence of Soot Mixing State on Aerosol Light Absorption and Single
504 Scattering Albedo during Air Mass Aging at a Polluted Regional Site in Northeastern
505 China." Journal of Geophysical Research Atmospheres 114(11):1–20, 2009.
506 Dentener, F. S., Kinne, T., Bond, O., Boucher, J., Cofala, S., Generoso, P., Ginoux, S., Gong,
507 J., J., Hoelzemann, A., Ito, L., Marelli, J., E., Penner, J., P., Putaud, C., Textor, M.,
508 Schulz, G., R., Van Der Werf, and J., Wilson.: "Emissions of Primary Aerosol and
509 Precursor Gases in the Years 2000 and 1750 Prescribed Data-Sets for AeroCom."
510 Atmospheric Chemistry and Physics 6(12):4321–44, 2006.
511 Dong, X., and J. S., Fu.: "Understanding Interannual Variations of Biomass Burning from
512 Peninsular Southeast Asia, Part II: Variability and Different Influences in Lower and
513 Higher Atmosphere Levels." Atmospheric Environment 115:9–18, 2015.
514 Fadnavis, S., T., Chakraborty, S., D., Ghude, G., Beig, and P., E., Raj.: "Modulation of
515 Cyclone Tracks in the Bay of Bengal by QBO." Journal of Atmospheric and Solar-
516 Terrestrial Physics 73(13):1868–75, 2011.
517 Fadnavis, S., K., Semeniuk, L., Pozzoli, M., G., Schultz, S. D., Ghude, S., Das, and R.,
518 Kakatkar.: "Transport of Aerosols into the UTLS and Their Impact on the Asian
519 Monsoon Region as Seen in a Global Model Simulation." Atmospheric Chemistry and
520 Physics 13(17):8771–86. 2013.
521 Fadnavis, S., G., Kalita, K. R., Kumar, B., Gasparini, and J. -L. F., Li.: "Potential Impact of
522 Carbonaceous Aerosol on the Upper Troposphere and Lower Stratosphere (UTLS) and

https://doi.org/10.5194/acp-2021-494
Preprint. Discussion started: 18 June 2021

Precipitation during Asian Summer Monsoon in a Global Model Simulation." Atmospheric Chemistry and Physics 17(18):11637–54, 2017.

Fadnavis, S., Müller, R., Kalita, G., Rowlinson, M., Rap, A., Li, J.-L. F., Gasparini, B., and Laakso, A.: "The impact of recent changes in Asian anthropogenic emissions of SO_2 on sulfate loading in the upper troposphere and lower stratosphere and the associated radiative changes." Atmos. Chem. Phys., 19, 9989–10008, https://doi.org/10.5194/acp-19-9989-2019, 2019.

Fadnavis, S., Sioris, C. E, Wagh, N., Chattopadhyay, R., Tao, M., Chavan, P., Chakroborty, T.: "A rising trend of double tropopause s over South Asia in a warming environment: Implications for moistening of the lower stratosphere." Int J Climatol. 2021;41, :E200–E215, DOI: 10.1002/joc.6677, 2021.

Fisher, J., A. D. J. Jacob, Q., Wang, R., Bahreini, C. C., Carouge, M. J. Cubison, J. E. Dibb, T., Diehl, J. L., Jimenez, E. M., Leibensperger, Z., Lu, Marcel, B. J. M., Havala, O. T. Pye, P. K., Quinn, S., Sharma, D. G., Streets, A., Donkelaar, and R. M., Yantosca.: "Sources, Distribution, and Acidity of Sulfate-Ammonium Aerosol in the Arctic in Winter-Spring." Atmospheric Environment 45(39):7301–18, 2011.

Gettelman, A. P., M., Piers, M., Fujiwara, Q., Fu, H., Vömel, L. K., Gohar, C., Johanson, and M., Ammerman.: "Radiation Balance of the Tropical Tropopause Layer." Journal of Geophysical Research: Atmospheres 109(7):1–12, 2004.

Giglio, L.,: "MODIS Collection 6 Active Fire Product User's Guide Revision A." Unpublished Manuscript, Department of Geographical Sciences, University of Maryland.[Link] (March):64, 2015.

Guenther, A.: "A Global Model of Natural Volatile Organic Compound Emissions." Journal of Geophysical Research 100(D5):8873–92, 1995.

Guha, A., B., Kumar De, P., Dhar, T., Banik, M., Chakraborty, R., Roy, A., Choudhury,

https://doi.org/10.5194/acp-2021-494
Preprint. Discussion started: 18 June 2021

548 Mukunda M. Gogoi, S. S., Babu, and K. Krishna Moorthy.: "Seasonal Characteristics of
549 Aerosol Black Carbon in Relation to Long Range Transport over Tripura in Northeast
550 India." Aerosol and Air Quality Research 15(3):786–98, 2015.
551 Guhathakurta, P., and M., Rajeevan.: "Trends in the Rainfall Pattern over India."
552 International Journal of Climatology 28(11):1453–69, 2008.
553 Hooghiem, Joram J.D., Maria Elena Popa, Thomas Röckmann, Jens Uwe Groob, Ines
554 Tritscher, Rolf Müller, Rigel Kivi, and Huilin Chen. 2020. "Wildfire Smoke in the
555 Lower Stratosphere Identified by in Situ CO Observations." Atmospheric Chemistry and
556 Physics 20 (22): 13985–3. https://doi.org/10.5194/acp-20-13985-2020, 2020.
557 Khaykin, S. B., Legras, S., Bucci, P., Sellitto, L., Isaksen, F., Tencé, S., Bekki, A., B., L.,
558 Rieger, D., Zawada, J., Jumelet, and S., Godin-Beekmann.: "The 2019/20 Australian
559 Wildfires Generated a Persistent Smoke-Charged Vortex Rising up to 35 Km Altitude."
560 Communications Earth & Environment 1, 22. https://doi.org/10.1038/s43247-020-
561 00022-5, 2020.
562 Lamarque, J., T., Bond, V., Eyring, C., Granier, A., Heil, Z., Klimont, D., Lee, C., Liousse,
563 A., Mieville, B., Owen, M., G., Schultz, D., Shindell, S., J., Smith, E., Stehfest, J.,Van
564 Aardenne, O.,R., Cooper, M., Kainuma, N., Mahowald, J., R.,McConnell, V., Naik, K.,
565 Riahi, and D., Vuuren.: "Historical (1850-2000) Gridded Anthropogenic and Biomass
566 Burning Emissions of Reactive Gases and Aerosols: Methodology and Application."
567 Atmospheric Chemistry and Physics 10(15):7017–39, 2010.
568 Lau, W., Kim, M-k., & Kim, K.: "Asian summer monsoon anomalies induced by aerosol
569 direct forcing: The role of the Tibetan Plateau." Climate Dynamics. 26. 855-864.
570 10.1007/s00382-006-0114-z, 2006.
571 Lestrelin, H., Legras, B., Podglajen, A., and Salihoglu, M.: Smoke-charged vortices in the
572 stratosphere generated by wildfires and their behaviour in both hemispheres: comparing

https://doi.org/10.5194/acp-2021-494
Preprint. Discussion started: 18 June 2021

573 Australia 2020 to Canada 2017, Atmos. Chem. Phys., 21, 7113–7134,
574 https://doi.org/10.5194/acp-21-7113-2021, 2021.
575 Lin, C., Y. C., Zhao, X., Liu, N. H., Lin, and W. N., Chen.: "Modelling of Long-Range
576 Transport of Southeast Asia Biomass-Burning Aerosols to Taiwan and Their Radiative
577 Forcings over East Asia." Tellus, Series B: Chemical and Physical Meteorology 66(1),
578 2014.
579 Li, Z., Yang, S., He, B., and Hu, C.,: Intensified Springtime Deep Convection over the South
580 China Sea and the Philippine Sea Dries Southern China, Scientific Reports, 6, Article
581 number: 30470, 2016.
582 Matson, M., and J., Dozier.: "Identification of Subresolution High Temperature Sources
583 Using a Thermal IR Sensor." Photogrammetric Engineering and Remote Sensing
584 47(9):1311–18, 1981.
585 Meehl, G. A., J., Arblaster, and W. D., Collins.: "Effects of Black Carbon Aerosols on the
586 Indian Monsoon." Journal of Climate 21(12):2869–82, 2008.
587 Mhawish, A. T., Banerjee, M., Sorek-Hamer, A., Lyapustin, D., Broday, and R., Chatfield.:
588 "Comparison and Evaluation of MODIS Multi-Angle Implementation of Atmospheric
589 Correction (MAIAC) Aerosol Product over South Asia." Remote Sensing of
590 Environment 224(February 2018):12–28, 2019.
591 Mieville, A., C., Granier, C., Liousse, B., Guillaume, F., Mouillot, J. F., Lamarque, J. M.,
592 Grégoire, and G., Pétron.: "Emissions of Gases and Particles from Biomass Burning
593 during the 20th Century Using Satellite Data and an Historical Reconstruction."
594 Atmospheric Environment 44(11):1469–77, 2010.
595 Murugavel, P., S. D., Pawar, and V., Gopalakrishnan.: "Trends of Convective Available
596 Potential Energy over the Indian Region and Its Effect on Rainfall." International
597 Journal of Climatology 32(9):1362–72, 2012.

https://doi.org/10.5194/acp-2021-494
Preprint. Discussion started: 18 June 2021

598 Nguyen, H. N., Bengt, G., Martinsson, J. B., Wagner, E., Carlemalm, M., Ebert, S.,
599 Weinbruch, C., A. M., Brenninkmeijer, J., Heintzenberg, M., Hermann, T., Schuck, P.,
600 F. J., van Velthoven, and A., Zahn.: "Chemical Composition and Morphology of
601 Individual Aerosol Particles from a CARIBIC Flight at 10 Km Altitude between 50°N
602 and 30°S." Journal of Geophysical Research Atmospheres 113(23):1–12, 2008.
603 Oman, L., D., Waugh, S., Pawson, R. S., Stolarski, and J. E., Nielsen.: "Understanding the
604 Changes of Stratospheric Water Vapor in Coupled Chemistry-Climate Model
605 Simulations." Journal of the Atmospheric Sciences 65(10):3278–91, 2008.
606 Oshima, N., Y., Kondo, N., Moteki, N., Takegawa, M., Koike, K., Kita, H., Matsui, M.,
607 Kajino, H., Nakamura, J., S., Jung, and Y., J., Kim.: "Wet Removal of Black Carbon in
608 Asian Outflow: Aerosol Radiative Forcing in East Asia (A-FORCE) Aircraft
609 Campaign." Journal of Geophysical Research Atmospheres 117(3):1–24, 2012.
610 Peterson, D. A., J. R., Campbell, Edward, J. H., Michael, D. F., George, P. K., J. H., Cossuth,
611 and Matthew, T. D.,: "Wildfire-Driven Thunderstorms Cause a Volcano-like
612 Stratospheric Injection of Smoke." Npj Climate and Atmospheric Science 1(1):1–8,
613 2018.
614 Randel, W., J. M., Park, L., Emmons, D., Kinnison, P., Bernath, Kaley, A., Walker, C. B.,
615 and H., Pumphrey.: "Asian Monsoon Transport of Pollution to the Stratosphere."
616 Science 328(5978):611–13, 2010.
617 Rieger L A., Malinina E. P., Rozanov .i V., Burrows J. P., Bourassa A. E., and Degenstein D.
618 A., A study of the approaches used to retrieve aerosol extinction, as applied to limb
619 observations made by OSIRIS and SCIAMACHY, Atmos. Meas. Tech., 11, 3433–3445,
620 2018, https://doi.org/10.5194/amt-11-3433-2018.
621 Riese, M., F., Ploeger, A., Rap, B., Vogel, P., Konopka, M., Dameris, and P., Forster.: Impact
622 of uncertainties in atmospheric mixing on simulated UTLS composition and related

https://doi.org/10.5194/acp-2021-494
Preprint. Discussion started: 18 June 2021

radiative effects, J. Geophys. Res., 117, D16305, doi:10.1029/2012JD017751, 2012.

Schill, G. P., K. D., Froyd, H., Bian, A., Kupc, C., Williamson, C. A., Brock, E., Ray, R. S., Hornbrook, A. J., Hills, E. C., Apel, M., Chin, P. R., Colarco, and D. M., Murphy.: "Widespread Biomass Burning Smoke throughout the Remote Troposphere." Nature Geoscience 13(6):422–27, 2020.

Schultz, M. G., A., Heil, J. J., Hoelzemann, A., Spessa, K., Thonicke, J., G., Goldammer, Alexander, C. H., J. M. C., Pereira, and M., Bolscher.: "Global Wildland Fire Emissions from 1960 to 2000." Global Biogeochemical Cycles 22(2):1–17, 2008.

Sherwood, S., V., Dixit, and C., Salomez.: "The Global Warming Potential of Near-Surface Emitted Water Vapour." Environmental Research Letters 13(10), 2018.

Shindell, D., T. M., Chin, F., Dentener, R. M., Doherty, G., Faluvegi, A. M., Fiore, P., Hess, D. M., Koch, I. A., MacKenzie, M. G., Sanderson, M. G., Schultz, M., Schulz, D. S., Stevenson, H., Teich, C., Textor, O., Wild, D., J., Bergmann, I., Bey, H., Bian, C., Cuvelier, B. N., Duncan, G., Folberth, L. W., Horowitz, J., Jonson, J. W., Kaminski, E., Marmer, R., Park, K. J., Pringle, S., Schroeder, S., Szopa, T., Takemura, G., Zeng, T. J., Keating, and A., Zuber.,: "A Multi-Model Assessment of Pollution Transport to the Arctic." Atmospheric Chemistry and Physics 8(17):5353–72, 2008.

Singh, N., V., Murari, M., Kumar, S., C., Barman, and T., Banerjee.: "Fine Particulates over South Asia: Review and Meta-Analysis of PM2.5 Source Apportionment through Receptor Model." Environmental Pollution 223:121–36, 2017.

Singh, P., P., Sarawade, and B., Adhikary.: "Transport of Black Carbon from Planetary Boundary Layer to Free Troposphere during the Summer Monsoon over South Asia." Atmospheric Research 235(October 2019):104761, 2020.

Singh, P., P., Sarawade, and B., Adhikary.: "Carbonaceous Aerosol from Open Burning and Its Impact on Regional Weather in South Asia." Aerosol and Air Quality Research

https://doi.org/10.5194/acp-2021-494
Preprint. Discussion started: 18 June 2021

20(3):419–31, 2020.

Stier, P., J. Feichter, S., Kinne, S., Kloster, E., Vignati, J., Wilson, L., Ganzeveld.: "The Aerosol-Climate Model ECHAM5-HAM." Atmospheric Chemistry and Physics 5 (4): 1125–56. https://doi.org/10.5194/acp-5-1125-2005, 2005.

Streets, D. G., K. F., Yarber, J. H., Woo, and G. R., Carmichael.: "Biomass Burning in Asia: Annual and Seasonal Estimates and Atmospheric Emissions." Global Biogeochemical Cycles 17(4), 1099, doi:10.1029/2003GB002040, 2003.

Talukdar, S., S., Jana, A., Maitra, and M. M., Gogoi.: "Characteristics of Black Carbon Concentration at a Metropolitan City Located near Land-Ocean Boundary in Eastern India." Atmospheric Research 153(October 2017):526–34, 2015.

Tegen, I. D., Neubauer, S., Ferrachat, C., Drian, I., Bey, N., Schutgens, P., Stier, Duncan, W., P. T., Stanelle, H., Schmidt, S., Rast, H., Kokkola, M., Schultz, Sabine S. N., Daskalakis, S., Barthel, B., Heinold, and U., Lohmann.: "The Global Aerosol-Climate Model Echam6.3-Ham2.3 -Part 1: Aerosol Evaluation." Geoscientific Model Development 12(4):1643–77, 2019.

Thomas, A., C., Sarangi, and V. P., Kanawade.: "Recent Increase in Winter Hazy Days over Central India and the Arabian Sea." Scientific Reports 9(1):1–10, 2019.

Val Martin, M., Logan, J. A., Kahn, R. A., Leung, F.-Y., Nelson, D. L., and Diner, D. J.: Smoke injection heights from fires in North America: analysis of 5 years of satellite observations, Atmos. Chem. Phys., 10, 1491–1510, https://doi.org/10.5194/acp-10-1491-2010, 2010.

Van Der Werf, G. R., J. T., Randerson, L., Giglio, G. J., Collatz, P. S., Kasibhatla, and A. F., Arellano.: "Interannual Variability in Global Biomass Burning Emissions from 1997 to 2004." Atmospheric Chemistry and Physics 6(11):3423–41, 2006.

Wang, S. H., N. H., Lin, M. D., Chou, and J. H., Woo.: "Estimate of Radiative Forcing of

https://doi.org/10.5194/acp-2021-494
Preprint. Discussion started: 18 June 2021

673 Asian Biomass-Burning Aerosols during the Period of TRACE-P." Journal of
674 Geophysical Research Atmospheres 112(10):1–17, 2007.
675 Wang, S. H., Ellsworth, J. W., Holben, B. N., S. C., Tsay, N. H., Lin, D., Giles, Sebastian, A.
676 S., S. J., Xuan, A., Nguyen, T., Hsiao, W. N., Chen, T. H,. Lin, S., Buntoung, S. C., and
677 W., Wiriya.: "Vertical Distribution and Columnar Optical Properties of Springtime
678 Biomass- Burning Aerosols over Northern Indochina during 2014 7-SEAS Campaign."
679 Aerosol and Air Quality Research 15(5):2037–50, 2015.
680 Wang, T., Q., Zhang, M., Kuilman, and A., Hannachi.: "Response of Stratospheric Water
681 Vapour to CO2 Doubling in WACCM." Climate Dynamics 54(11–12):4877–89, 2020.
682 Weigel, R., Mahnke, C., Baumgartner, M., Dragoneas, A., Vogel, B., Ploeger, F., Viciani, S.,
683 D'Amato, F., Bucci, S., Legras, B., Luo, B., and Borrmann, S.: In-Situ observation of
684 New Particle Formation in the upper troposphere/lower stratosphere of the Asian
685 Monsoon Anticyclone, Atmos. Chem. Phys. Discuss. [preprint],
686 ttps://doi.org/10.5194/acp-2020-1158, in review, 2020.
687 Wu, J., S., Kong, F., Wu, Y., Cheng, S., Zheng, Q., Yan, H., Zheng, G., Yang, M., Zheng, D.,
688 Liu, D., Zhao, and S., Qi.: "Estimating the Open Biomass Burning Emissions in Central
689 and Eastern China from 2003 to 2015 Based on Satellite Observation." Atmospheric
690 Chemistry and Physics 18(16):11623–46, 2018.
691 Xie, F., W., Tian, X., Zhou, J., Zhang, Y., Xia, and J., Lu.: "Increase in Lower Stratospheric
692 Water Vapor in the Past 100 Years Related to Tropical Atlantic Warming." Geophysical
693 Research Letters 47(22), 2020.
694 Zhang, X., J., Liu, H., Han, Y., Zhang, Z., Jiang, H., Wang, L., Meng, Y. C., Li, and Y., Liu.:
695 "Satellite-Observed Variations and Trends in Carbon Monoxide over Asia and Their
696 Sensitivities to Biomass Burning." Remote Sensing 12(5), 2020.

https://doi.org/10.5194/acp-2021-494
Preprint. Discussion started: 18 June 2021

Atmospheric Chemistry and Physics Discussions

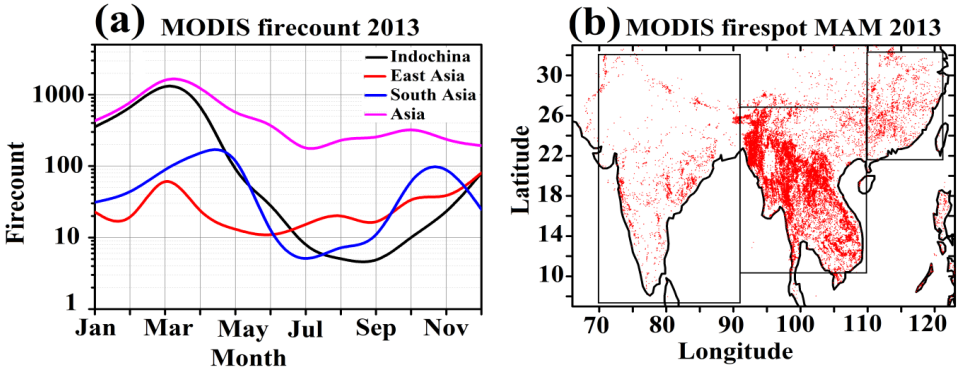

Figure 1: (a) Monthly mean distribution of MODIS fire count averaged over Indochina (91°E-107°E, 10°N-27°N), East Asia (108°E-123°E, 22°N-32°N), South Asia (70°E-90°E, 8°N-32°N) and Asia (60°E-130°E, 10°S-50°N) (b) spatial distribution of seasonal mean fire spot over South Asia, Indochina and East Asia. Boxes in Figure (b) indicate the boundaries of South Asia, Indochina, and East Asia.

https://doi.org/10.5194/acp-2021-494
Preprint. Discussion started: 18 June 2021

Atmospheric Chemistry and Physics Discussions

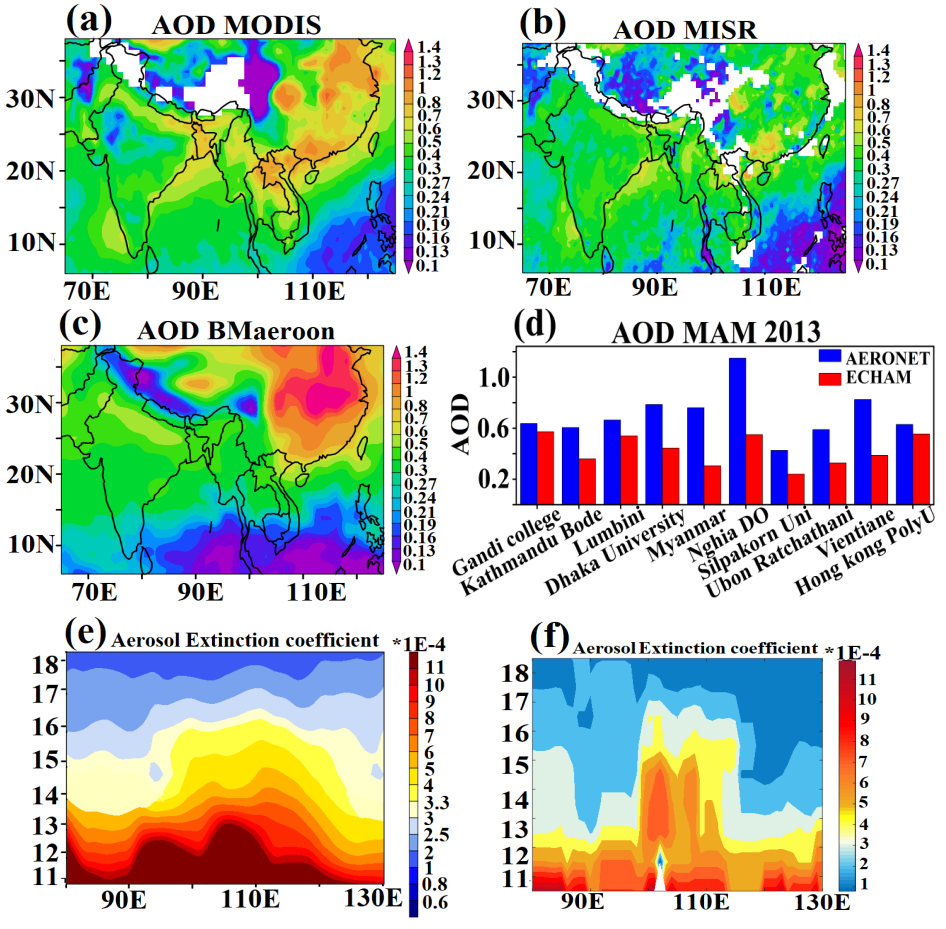

Figure 2: (a) Seasonal mean aerosol optical depth (AOD) for 2013 from MODIS, (b) same as (a) but from MISR, (c) same as (a) but from ECHAM6 - HAMMOZ BMaeroon simulation. (d) Comparison of simulated AOD (from BMaeroon) averaged for spring 2013 with AERONET observations at Gandhi college:25.81°N-85.12°E, Kathmandu Bode:27.68°N-85.39°E, Lumbini:27.49°N-83.28°E, Dhaka University:23.72°N-90.39°E, Myanmar:16.86°N-96.15°E, Nghia Do:21.04°N-105.80°E, Silpakorn University:13.81^{0}N-100.05^{0}E, Ubon Ratchathani:15.24^{0}N-104.87^{0}E, Vientiane:17.99^{0}N-102.57°E, Hong Kong PolyU:22.30°N-114.18°E, (e) simulated (BMaeroon) aerosol extinction coefficient (865 nm) (km^{-1}), averaged for 12°N -30°N and spring 2013 (f) same as (e) but from OSIRIS measurements (750 nm).

https://doi.org/10.5194/acp-2021-494
Preprint. Discussion started: 18 June 2021

Atmospheric Chemistry and Physics Discussions

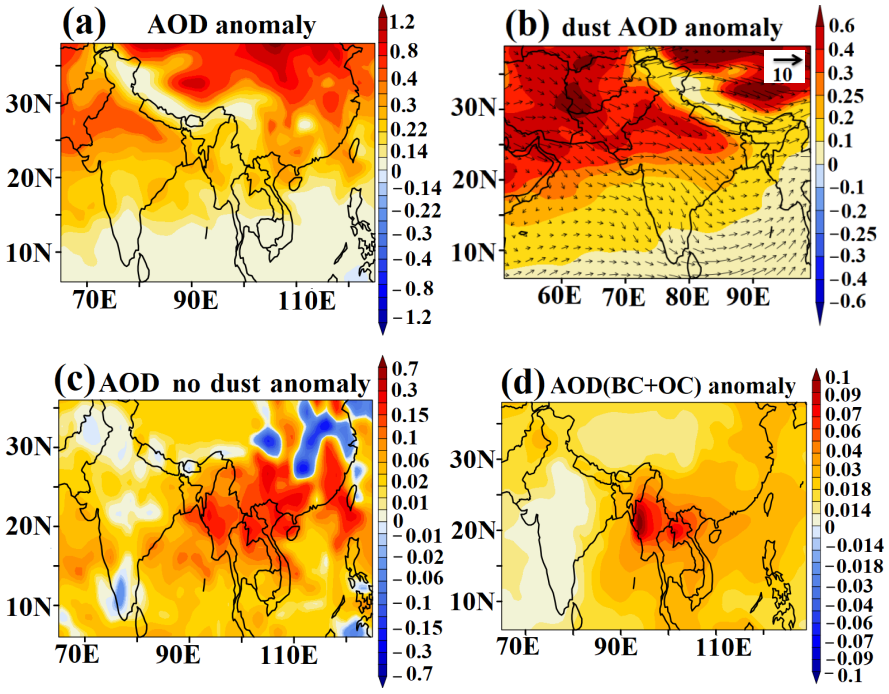

Figure 3. Seasonal mean anomalies of ECHAM6-HAMMOZ simulated (BMaeroon - BMaerooff) (a) AOD, (b) dust AOD, (c) same as figure (a) but without dust AOD, (d) BC-AOD and OC-AOD, together.

https://doi.org/10.5194/acp-2021-494
Preprint. Discussion started: 18 June 2021

Atmospheric Chemistry and Physics Discussions

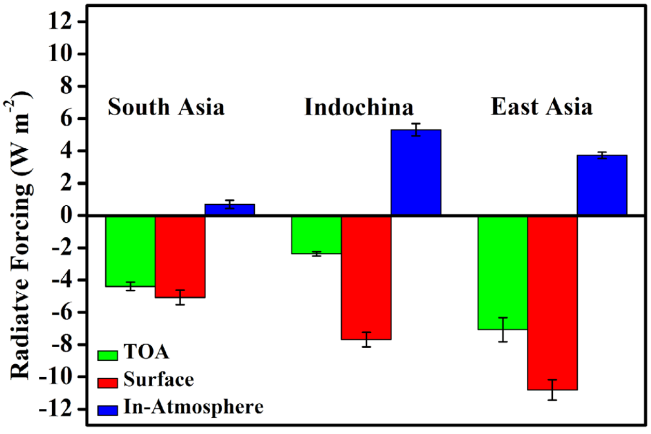

Figure 4. Seasonal mean anomalies of Radiative Forcing ($W.m^{-2}$) from ECHAM6-HAMMOZ simulations (BMaeroon - BMaerooff) at the TOA, surface, and in-atmosphere (TOA - Surface) for spring 2013 averaged over South Asia, Indochina, and East Asia.

https://doi.org/10.5194/acp-2021-494
Preprint. Discussion started: 18 June 2021

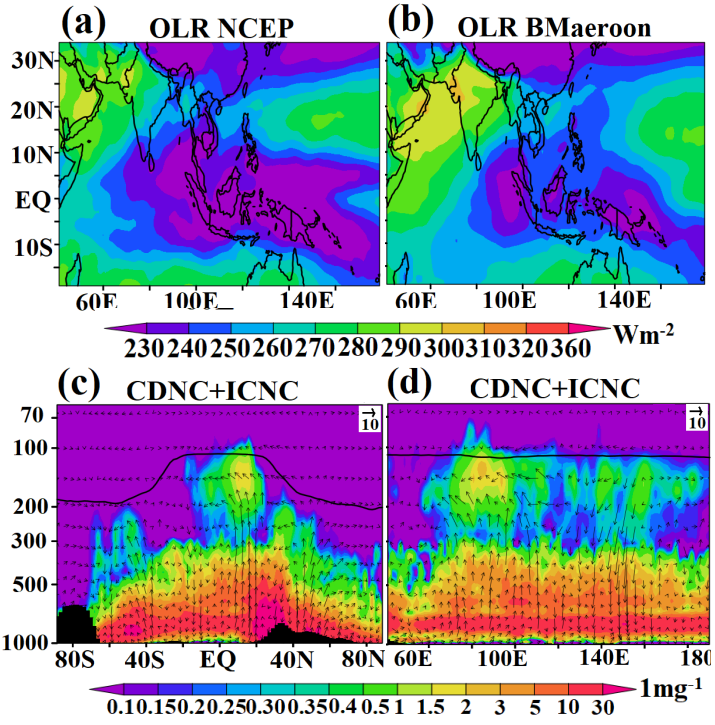

Figure 5: (a) Seasonal mean distribution of Outgoing Longwave Radiation (OLR) (W m^{-2}) from NCEP reanalysis-2 data for spring 2013, (b) same as (a) but from the ECHAM6-HAMMOZ simulations (BMaeroon). Vertical distribution of cloud droplet number concentration (CDNC) and ice crystal number concentration (ICNC) (1 mg^{-1}) averaged for spring 2013 from ECHAM6-HAMMOZ simulations (BMaeroon) (c) latitude-pressure section (average for 85^0E-140^0E) and (d) longitude-pressure section (average for 10^0S - 10^0N).

https://doi.org/10.5194/acp-2021-494
Preprint. Discussion started: 18 June 2021

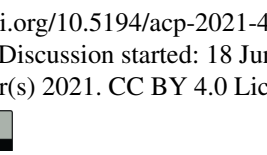

Atmospheric Chemistry and Physics Discussions

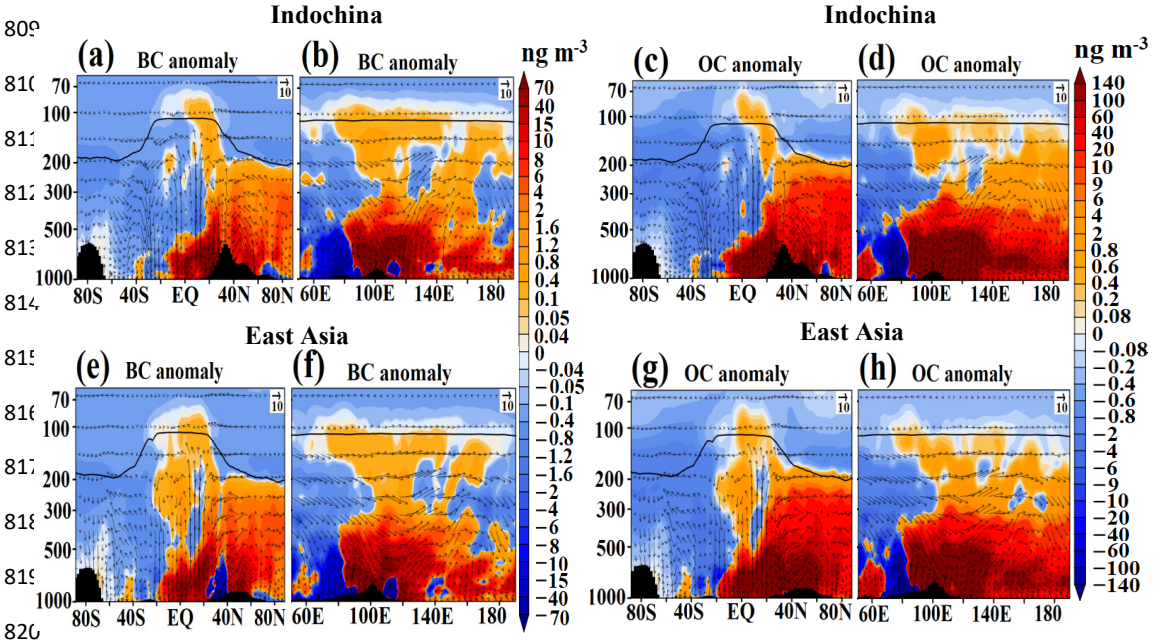

Figure 6. Vertical cross-section of anomalies of BC (ng m^{-3}) (BMaeroon – Bmaerooff) averaged for the spring 2013 and (a) latitude-pressure section (averaged for 91°E-107°E), (b) longitude-pressure section (averaged for 18°N-24°N). (c-d) is the same as (a-b) but for OC. (e) same as (a) but averaged over 105°E-125°E, (f) same as (b) but averaged for 18°N-24°N. (g-h) same as in (e-f) but for OC. The arrows in (a-f) indicate winds in m s^{-1}. The black vertical bar shows the topography and the black line indicates the tropopause.

https://doi.org/10.5194/acp-2021-494
Preprint. Discussion started: 18 June 2021

Atmospheric Chemistry and Physics Discussions

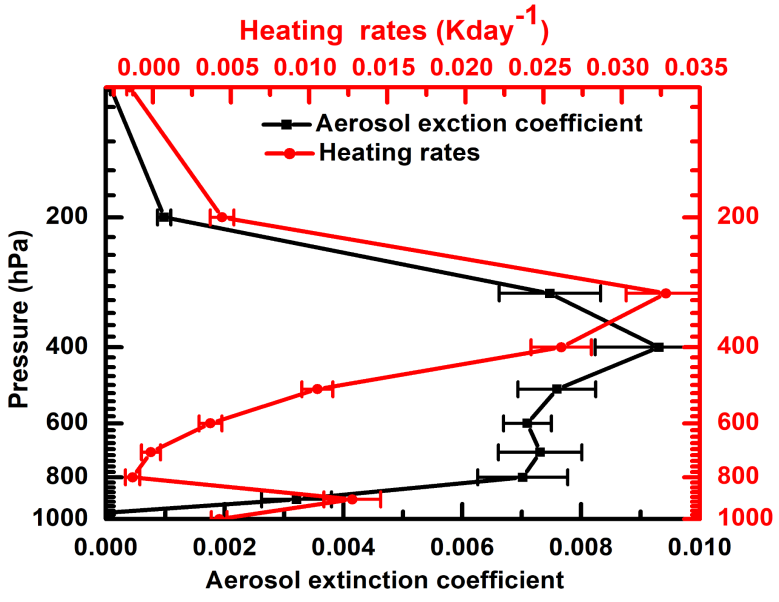

Figure7: Vertical profile of anomalies of extinction (km^{-1}) and heating rate (K day^{-1}) over the Arctic region (65°N-85°N) from the ECHAM6-HAMMOZ simulations (BMaeroon - BMaerooff). The horizontal lines indicate standard deviation within the 10 members of the different initial conditions.

https://doi.org/10.5194/acp-2021-494
Preprint. Discussion started: 18 June 2021

Atmospheric Chemistry and Physics Discussions

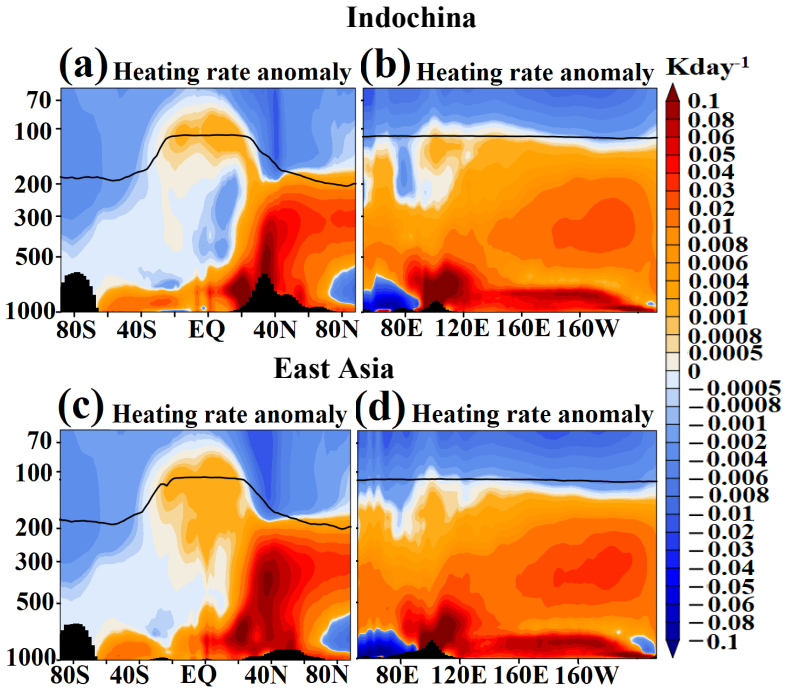

Figure 8. Vertical section of heating rate anomalies (K day^{-1}) for spring season 2013 from ECHAM6-HAMMOZ simulations (BMaeroon - BMaerooff) (a) latitude-pressure section averaged for 91°E-107^{0}E, (b) longitude-pressure section averaged for 18^{0}N-24^{0}N. (c) same as (a) but averaged for 108°E-123^{0}E. (d) same as (b) but averaged for 22^{0}N-27^{0}N.

https://doi.org/10.5194/acp-2021-494
Preprint. Discussion started: 18 June 2021

Atmospheric Chemistry and Physics Discussions

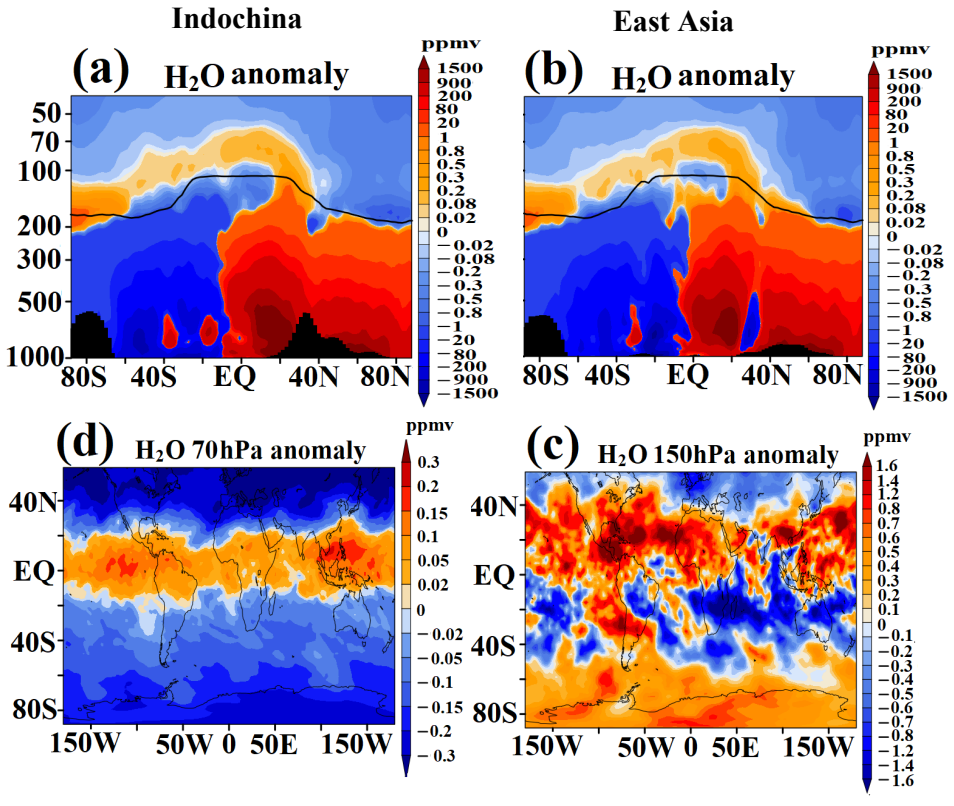

Figure 9. Vertical and horizontal distribution of anomalies of water vapour (ppmv) for spring 2013 from the ECHAM6-HAMMOZ simulations (BMaeroon - BMaerooff) (a) latitude-pressure cross-section averaged for 91°E-107°E, (b) longitude-pressure cross-section averaged over 108°E-123°E, at (c) 150 hPa level, and (d) 70 hPa level.